THE JOURNAL OF PHYSICAL CHEMISTRY C

Article

pubs.acs.org/JPCC

Interfacial Bonding and Morphological Control of Electropolymerized Polythiophene Films on ZnO

Wenchun Feng,[†] Alan S. Wan,[‡] and Eric Garfunkel*,[†]

[†]Department of Chemistry and Chemical Biology, Rutgers University, Piscataway, New Jersey 08854, United States

[‡]Evans Analytical Group, East Windsor, New Jersey 08520, United States

Supporting Information

ABSTRACT: Integrating polymers with inorganic nanostructures is difficult due to wetting and surface energy considerations. In this paper, we developed an electropolymerization method to grow conformal polymers on high aspect ratio nanostructures. Our method is shown to improve the polymer filling rate inside the nanostructures and can be used in the development of efficient hybrid solar cells. As an example, we have studied the hybrid system of electropolymerized polythiophene (e-PT) on ZnO planar and nanorod substrates using surface characterization methods. Although unsubstituted polythiophene is not the ideal polymer material for high efficiency solar cells, it is an excellent choice for studying basic bonding and morphology in hybrid structures. We find that e-PT is covalently bound to the polar ZnO planar substrate via a Zn−S bond, adopting an upright geometry. By contrast, no strong covalent bonding was observed between e-PT and ZnO nanorods that consist of nonpolar ZnO surfaces predominantly. We manipulated the polymer morphology along the ZnO nanorods by tuning the polarity of the solvent used in electropolymerization. Our electropolymerization approach to integrate the organic and inorganic phases aims at understanding the chemistry at the interface, and the electronic and morphological properties of the system. This work should be generally applicable to other conjugated polymers and nanostructures, and it contributes to an understanding of organic−inorganic interfaces and structures that may be advantageous to a range of electronic/photonic applications.

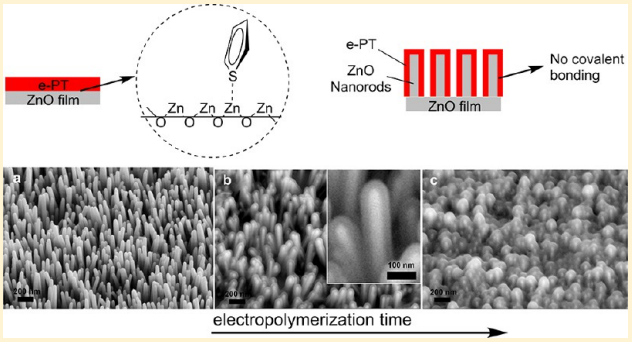

1. INTRODUCTION

Conducting conjugated polymers have received considerable attention in a wide range of electronic and optoelectronic technologies, including organic photovoltaics (OPVs), organic light emitting diodes (OLEDs), organic thin film transistors, and organic memory devices.[1] In particular, p-type conducting polymer polythiophene (PT) and its derivatives [one of the most notable is poly(3-hexylthiophene), P3HT] have been among the most extensively studied materials for OPVs because of their optical properties, relatively high hole mobilities, synthetic versatility, and potential for cost-effective mass production.

One class of next-generation PVs employs an n-type inorganic nanostructure as the electron acceptor and a p-type conducting polymer as the electron donor. This hybrid architecture offers several potential advantages over its all-organic counterparts: considerably higher electron mobility in the inorganic phase, better morphological stability, and low-cost fabrication of the inorganic nanostructure. An ideal hybrid solar cell should have an optimized nanostructure enabling efficient exciton diffusion, maximized interfacial area for charge separation, and direct pathways for charge transfer.[2] High density ZnO nanorod arrays interdigitated with PT in which the two phases are in intimate contact, satisfactorily meets the requirement of such an ideal architecture. Herein, ZnO nanorods were chosen as the electron acceptor because of their relatively high electron mobility and an appropriate band alignment with PT at the interface. From a practical manufacturing perspective, ZnO has the advantages of high natural abundance, low cost, small environmental impact, and nontoxicity. Unsubstituted PT was chosen as the p-type conducting polymer because it serves as a model system with a thiophene backbone and no side chains. Although PT is far from the ideal polymer system for high efficiency OPVs,[3] we are taking advantage of its simple molecular construction and ease of electropolymerization as our model polymer as opposed to more complicated polymer structures.

The exciton diffusion length in a conducting polymer system is typically less than 10 nm.[4] For efficient exciton diffusion to the organic−inorganic interface, the ZnO rod-to-rod spacing should be twice the exciton diffusion length. This small length scale makes it challenging for complete polymer infiltration into the ZnO nanorods. Conventional methods involve spin-coating and thermal or solvent vapor annealing, with limited success at

Received: January 25, 2013
Revised: March 28, 2013
Published: April 1, 2013

   dx.doi.org/10.1021/jp400871g | J. Phys. Chem. C 2013, 117, 9852−9863

filling into the nanorod arrays.[5−7] An alternative method, such as chemical grafting of end-functionalized oligothiophenes and P3HT onto ZnO nanorods, has produced core−shell structures.[8] However, due to the nature of self-assembly, it is difficult to control the thickness of the polymer layer or grow polymer layers thicker than 20 nm. Integrating polymers into high-density arrays of ZnO nanorods to fabricate high quality core−shell and bulk heterojunction structures is a key motivating factor for this work.

Electropolymerization, where monomers in solution are polymerized onto the electrode surface to form oligomers and eventually polymers, is a logical pathway to enhance polymer infiltration because of its continuous and controllable surface-initiated polymerization nature. Monomers adsorbed onto the electrode prior to electropolymerization serve as anchor sites for subsequent polymer chain growth. Assuming adsorption to saturation coverage, conformal polymer growth along the electrode surface can be attained, and intimate contact between the electropolymerized-PT (e-PT) and the ZnO nanorods can be realized. The only requirement for electropolymerization is a sufficiently conductive electrode; this is adequately satisfied in our study.

Electropolymerization has recently been applied to the fabrication of efficient hybrid solar cells. Exemplary reports include e-P3HT/CdS nanorods,[9] e-P3HT/CdS/ZnO nanorods,[10] e-PEDOT [Poly(3,4-ethylenedioxythiophene)]/ZnO nanorods,[11] and e-P3HT[12] or e-PEDOT[13] on GaAs nanowires. However, fundamental and in-depth studies of the electropolymerized polymer/inorganic interface, most critical for the charge separation process, have been limited. Our X-ray photoelectron spectroscopy (XPS) studies shed light on the bonding nature, chemical structure, and molecular orientation of e-PT on ZnO planar and nanostructured substrates. These studies, in turn, serve as an important basis in helping develop a fundamental understanding of the charge separation that occurs at the organic−inorganic interface. We compare our results to adsorption studies of sulfur-containing molecules (alkylthiol,[14−17] thiophene,[18,19] and sexithiophene[20−22]) on ZnO surfaces.

Electropolymerization is controlled by a variety of parameters, among which we find that the polarity of the solvent exerts a strong influence on the e-PT film morphology along ZnO nanorods. Versatile manipulation of e-PT film morphology on ZnO nanorods can be achieved by tuning the polarity of the solvent, producing either a core−shell or bulk heterojunction (BHJ) structure. For the BHJ structure, XPS depth profiling shows that the polymer has completely infiltrated to the bottom of the nanorods upon thermal annealing.

Photovoltaic $J-V$ characterization was performed on e-PT/ZnO bilayer and BHJ devices. The BHJ devices incorporate a polymer overlayer on top of the nanorods, intended as an electron blocking layer for device improvement. However, as the electropolymerization produces thicker films such as this overlayer, the polymer structure becomes increasingly regiorandom which results in poor electronic properties such as lower carrier mobilities. Replacing this BHJ structure with a core−shell structure with thin e-PT films along ZnO nanorods should result in higher quality devices and is the focus for ongoing research.

2. EXPERIMENTAL METHODS

2.1. Materials. Zinc acetate dihydrate (99%, Aldrich), zinc nitrate hexahydrate (99%, Aldrich), ethanolamine (99%, Aldrich), hexamethylenetetramine (HMTA, 99%, TCI America), 2,2′-bithiophene (98%, TCI America), tetrabutylammonium hexafluorophosphate (Bu_4NPF_6, 98%, TCI America), 2-methoxyethanol (99%, Acros), dichloromethane (DCM, 99.8%, Acros), and acetonitrile (ACN, 99.8%, Aldrich) were used without further purification. Clevios HTL Solar PEDOT:PSS, poly(3,4-ethylenedioxythiophene):poly(styrenesulfonate), was purchased from Heraeus. ITO-coated glass slides (Delta Technologies and MTI Corporation) were subjected to successive 10 min ultrasonication in dichloromethane and acetone before being blown dried in a stream of nitrogen.

2.2. Synthesis of ZnO Planar and Nanorod Substrates. ZnO films were made by a sol−gel method. A 750 mM zinc acetate solution in 2-methoxyethanol with equal molar ratio of zinc acetate and ethanolamine was spin-coated at 2000 rpm for 30 s. Then the sol−gel films were annealed on a hot plate in air at 300 °C for 10 min. This sol−gel method afforded ZnO films that are ∼30 nm thick. For the synthesis of ZnO nanorods, the sol−gel prepared ZnO film was used as a seed layer. ZnO nanorods were grown from the ZnO planar substrate by a hydrothermal method in a Teflon-lined stainless steel reactor. The substrate was suspended and facing down in 12 mL solution of 25 mM zinc nitrate hexahydrate and 25 mM hexamethylenetetramine (HMTA) at 92.5 °C. The mechanism for the hydrothermal growth of ZnO nanorods is illustrated in the equations below:[23]

$$(CH_2)_6N_4 + 6H_2O \leftrightarrow 6HCHO + 4NH_3 \quad (1)$$

$$NH_3 + H_2O \leftrightarrow NH_4^+ + OH^- \quad (2)$$

$$Zn^{2+} + 2OH^- \leftrightarrow Zn(OH)_2 \leftrightarrow ZnO + H_2O \quad (3)$$

The as-grown ZnO nanorods were thoroughly rinsed with distilled water and dried in air.

2.3. Electropolymerization. Electrochemical experiments were carried out with a Princeton Applied Research VersaSTAT potentiostat. A three-electrode system was used. The working electrode was the ZnO substrate. The counter electrode was Pt gauze. The reference electrode was a Ag/Ag^+ nonaqueous reference electrode consisting of 0.01 M $AgNO_3$ and 0.1 M Bu_4NPF_6 in acetonitrile. All potentials reported in this paper were referenced to this Ag/Ag^+ reference electrode. The electrochemical cell contains ∼12 mL solution of 0.01−0.05 M 2,2′-bithiophene and 0.1 M Bu_4NPF_6 in DCM or ACN. Before electropolymerization, the solutions were deoxygenated by bubbling nitrogen through the solution for 10 min; a nitrogen overpressure was maintained throughout the experiment. PT can be electropolymerized onto the working electrode potentiodynamically (cycling potentials) or by potentiostatic methods (keeping the potential constant). The sample was then removed from the solution and rinsed with copious amount of solvent. The sample was reduced by a standby potential of −1 V (vs Ag/Ag^+ reference electrode) in a monomer-free electrolyte solution until the current was stable. The sample was again removed from solution and rinsed thoroughly.

2.4. Device Fabrication and Testing. The e-PT/ZnO samples were annealed at 300 °C in argon for 30 min. PEDOT:PSS was deposited from a solution which was spin-coated at 1000 rpm/s for 30 s and annealed in air on a hot plate at 120 °C for 3 min. This produced a PEDOT:PSS layer of ∼50 nm thickness. The top electrodes, ∼80 nm Ag with an electrode area of 0.03 cm^2, were thermally evaporated in vacuum with a

dx.doi.org/10.1021/jp400871g | J. Phys. Chem. C 2013, 117, 9852−9863

Scheme 1. Synthesis of ZnO Planar and Nanorod Substrates and Electropolymerization[a]

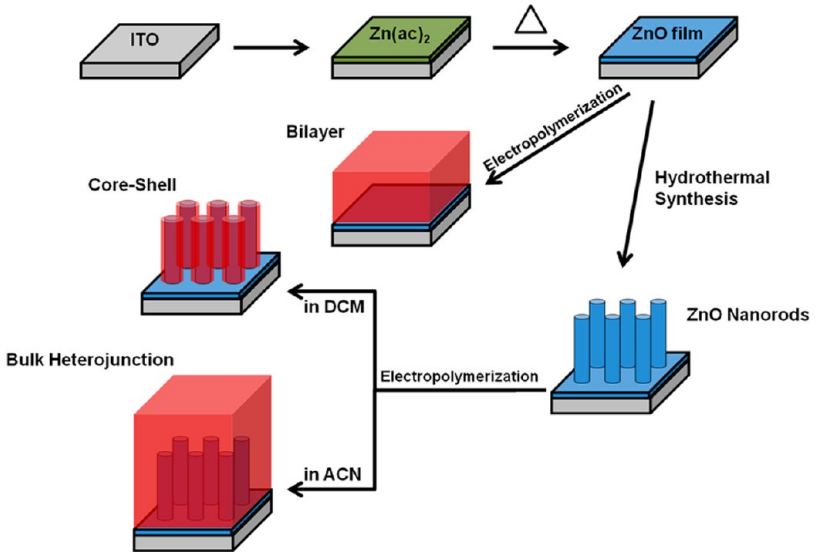

[a]DCM: dichloromethane. ACN: acetonitrile.

base pressure $\leq 1 \times 10^{-6}$ Torr. Photovoltaic $J-V$ characterization was carried out using a HP 4140B pA meter/DC voltage source under AM 1.5 illumination of 100 mW/cm^2 with a 300 W xenon solar simulator. A Labview program was used to control the solar simulator as well as the electrical characterization equipment; voltages between −1 V and 1 V were delivered to the solar cell with a step size of 10 mV.

2.5. Characterization Methods. A Thermo Scientific K-Alpha X-ray photoelectron spectroscopy system was used for XPS measurements. The photoelectron takeoff angle was typically 90°, and the X-ray source was monochromated Al Kα radiation (1486.3 eV). The binding energy was referenced to the adventitious C 1s peak at 285.0 eV. Shirley background subtraction was performed, and the spectra were fit with Gaussian/Lorentzian peaks using a minimum deviation curve fitting method (part of the Avantage software package). The surface composition of each species was determined by the integrated peak areas and the Scofield sensitivity factor provided by the Avantage software. Argon sputter depth profiling was performed using a 2 keV Ar^+ beam at high current density on an area of 2 × 2 mm^2. Under this condition, the estimated sputter rate (calibrated for Ta_2O_5) is 0.50 nm/s.

UPS data were collected with a He discharge source which produces resonant lines by capillary discharge at 21.2 eV (He I) and 40.8 eV (He II). The analyzer was a cylindrical mirror analyzer, and the pass energy was set to 10 eV. The energy resolution was determined to be ∼150 meV by the width of the Fermi step measured on clean Au. A negative bias of 4.8 V was applied to the sample to overcome the detector work function limitations when measuring the secondary electron energy cutoff.

UV−visible absorption spectra were recorded on a Shimadzu UV-3101PC UV−vis spectrophotometer. PL spectra were obtained on a Horiba Jobin Yvon Fluorolog-3 spectrofluorometer.

The morphology of the ZnO nanorods and e-PT was visualized by scanning electron microscopy (Zeiss Sigma Field Emission SEM).

3. RESULTS AND DISCUSSION

3.1. Overview of Synthesis Methods. The syntheses involved in this paper are of ZnO films, nanorods, and electropolymerization on various ZnO substrates (Scheme 1). ZnO films were prepared by a sol−gel technique. Compared to other synthesis methods, sol−gel has many advantages such as low material and equipment cost and ease of large-area fabrication. Subsequently, the as-prepared ZnO thin films serve as a seed layer for the hydrothermal synthesis of ZnO nanorods.

Although other techniques such as metal−organic chemical vapor deposition (MOCVD) or pulsed laser deposition (PLD) can be used to synthesize ZnO nanorods, hydrothermal synthesis has the cost-effective benefits of requiring a simple apparatus and offering a high throughput. More importantly, the as-grown ZnO nanorods adopt advantageous vertical alignment to the substrate if the nanorods and the substrate have minimal lattice mismatch.[24] ZnO nanorods grown on a ZnO seed layer are epitaxial and show preferential growth in a direction normal to the surface as evidenced by the very large intensity of the (002) diffraction peak in XRD (Supporting Information, Figure S1). The high nanorod density observed meets the desired high surface area structure that was initially proposed. Such a structure is needed for efficient charge separation in a hybrid organic−inorganic PV. ZnO nanorods have a polar Zn-terminated (0001) or O-terminated $(000\bar{1})$ tip and nonpolar mixed-terminated $(10\bar{1}0)$ sidewalls. The polar Zn-(0001) or O-$(000\bar{1})$ tip have higher energy than the nonpolar sidewalls, and thus either form complex surface structures or undergo reconstruction to reduce their electrostatic energy.[25] ZnO growth occurs favorably on the higher energy (0001) and $(000\bar{1})$ surfaces to reduce the overall free energy of the system, forming one-dimensional ZnO nanostructures.

Electropolymerization of PT is carried out on ZnO planar substrates or nanorod substrates. For electropolymerization on ZnO nanorod substrates, we can grow either core−shell structures or bulk heterojunction structures depending on the solvent used in the electrochemical solution. The mechanism

dx.doi.org/10.1021/jp400871g | J. Phys. Chem. C 2013, 117, 9852−9863

for electropolymerization of conjugated polymers on ZnO substrates is as follows: the monomers diffuse to and adsorb on ZnO surfaces. As electropolymerization begins, the monomers are electro-oxidized and produce radical cations. This is followed by the coupling of two radical cations, expulsion of H^+, and a repetition of this process, forming oligomers and eventually polymers.[26]

The high oxidation potential of unsubstituted thiophene is close to the degradation potential of e-PT. This results in the formation of many side products, cross-linking, and shortened conjugation length which is detrimental to charge transport. The usage of 2,2′-bithiophene decreases the polymerization potential by a significant 0.7 V; this helped guide our choice of monomer.[27] The required minimal oxidation potential for 2,2′-bithiophene is experimentally determined to be 0.80 V in acetonitrile and 0.90 V in dichloromethane (vs Ag/Ag^+ reference electrode). The 0.1 V difference in minimal oxidation potential is likely due to the different liquid junction potentials at the reference electrode in two different solvents. With a given solvent, the required minimal oxidation potential of e-PT formation on ZnO planar or nanorod substrates is the same. This is presumably because the unintentional doping (note that both zinc nitrate and HTMA are only of 99% purity) during hydrothermal synthesis is significant enough to produce highly doped ZnO nanorods with small electrical resistance.

Extensive optical and photoemission studies confirmed the formation of PT from electropolymerization. UV−vis absorption spectrum (Supporting Information, Figure S2) of the polymer film is typical for PT with absorption maxima at 524, 541, and 566 nm, with a 2.0 eV optical bandgap. PL spectrum (Supporting Information, Figure S2) was taken at an excitation wavelength of 488 nm and the emission maxima are at 619 and 665 nm, in agreement with published results.[28] Valence level UPS He II spectrum (Supporting Information, Figure S3) is a fingerprint spectrum for PT.[29] XPS studies verified the chemical composition of PT with the atomic ratio of carbon and sulfur at 4:1 and showed no sign of overoxidation from the electropolymerization process that would lead to degradation of electronic properties. Our XPS results will be discussed in more details in the following section.

3.2. Interfacial Bonding of e-PT/ZnO: XPS. The organic−inorganic interface is considered to be critical for charge separation and device performance. Herein, we carry out XPS studies on the interfacial bonding between e-PT and ZnO, which include both the ZnO planar substrates (Section 3.2.1) and ZnO nanorod substrates (Section 3.2.2).

3.2.1. e-PT/ZnO Planar Substrate. The XPS analysis depth from which meaningful information can be derived is less than 10 nm, thus the electrodeposited polymer film should be as thin as possible so that information about the interface can be discerned. To maximize the signal-to-noise ratio of various elements (carbon and sulfur from e-PT, zinc and oxygen from ZnO) at the interface, it would be best to have only one monolayer adsorbed across the entire substrate because further growth would attenuate the intensity of these interface species. In reality, the very beginning of electropolymerization is characterized by nucleation and growth into island-like deposits.[30] Therefore, it is highly unlikely that one monolayer adsorption with perfect coverage will occur. We have found that the best interface signal is achieved by electropolymerizing a very thin layer of e-PT on ZnO planar substrate at 1.0 V (0.2 V higher than the minimal oxidation potential) for only 0.4 s in a dilute 0.01 M monomer solution in acetonitrile. The mild potential, combined with short polymerization time in dilute solution, is successful in obtaining polymer films that give satisfactory XPS intensity without being too thick and obscuring information at the interface.

Theoretical cluster calculations[19] on thiophene adsorption shows that there are two possible bonding configurations of adsorbed thiophene on ZnO: S−Zn and C−Zn. The interaction between thiophene and O is considered to be energetically much less favorable. Our XPS study also focuses on the two possible bonding structures, S−Zn and C−Zn, at the interface.

The wide energy XPS spectrum of the electrodeposited PT film on a planar ZnO substrate (Figure 1a) confirms the

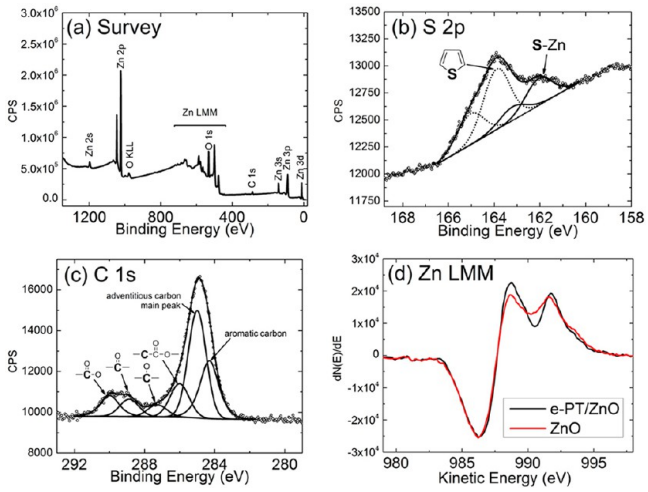

Figure 1. (a) Wide energy, (b) S 2p, and (c) C 1s XPS spectra of e-PT on ZnO planar substrate. (d) First-derivative Zn $L_3M_{4,5}M_{4,5}$ Auger spectrum of ZnO planar substrate with e-PT coverage (black line) and without e-PT coverage (red line).

chemical composition of the pure ZnO film. A detailed scan of the S 2p peak energy region from a PT/ZnO structure is shown in Figure 1b. Curve fitting suggests that there are two S 2p spin−orbit doublets, with the $2p_{3/2}$ peaks centered at 163.8 (dashed line) and 161.9 eV (solid line), respectively. Both of the doublets have a splitting of 1.2 eV, and the ratio of $2p_{3/2}$ to $2p_{1/2}$ peak areas can be fit to the expected 2:1. The higher binding energy peak at 163.8 eV is attributed to sulfur in thiophene. The lower binding energy peak at 161.9 eV is typical of sulfide,[31] which is presumably ZnS. By contrast, there is no sulfide peak present in the bulk PT film spectrum (Supporting Information, Figure S4), indicating that the sulfide peak originates from the interface. Sulfur in the sulfide form represents 31% of the total amount. Additionally, the lack of an oxidized S 2p peak, normally appearing at higher binding energy ∼168 eV,[32] indicates that the polymer film is not overoxidized under our mild oxidation conditions and there is no sulfur−oxygen bonding (which is deemed unfavorable by calculation).[19] The resolution and intensity of the 161.9 eV peak demonstrates the existence of sulfide bonding at the interface. It should be noted that the slope on which the S 2p peaks rest is part of a plasmon loss feature from the Zn 3s transition and is unrelated to the S 2p signal.

The C 1s (Figure 1c) can be interpreted as arising from aromatic α and β carbons from e-PT, as well as adventitious carbon. The main peak of adventitious carbon was referenced to 285.0 eV. Four higher binding energy peaks (286.0, 287.3,

dx.doi.org/10.1021/jp400871g | J. Phys. Chem. C 2013, 117, 9852−9863

Scheme 2. Molecular Geometry and Bonding Structure for e-PT on ZnO Planar Substrates at Different Coverages

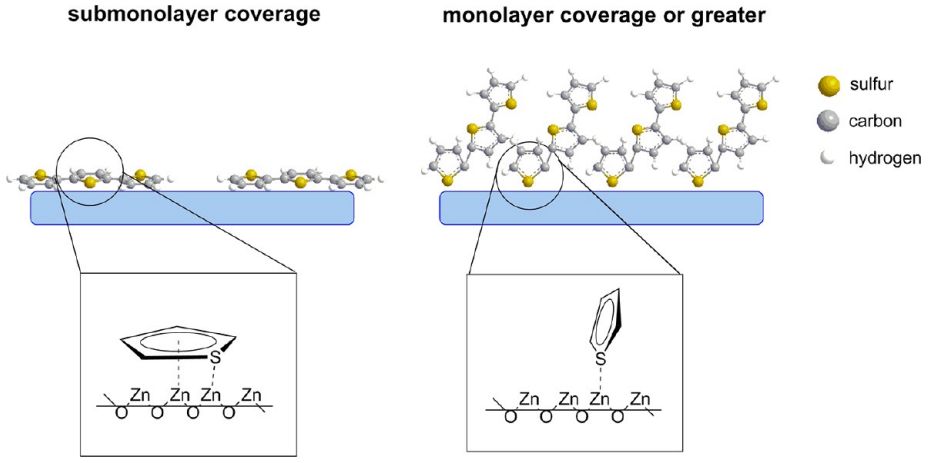

288.9, and 290.0 eV) are attributed to various oxidation states. Conjugated aromatic polymers such as PT may have a weak satellite with a binding energy that is 6−7 eV higher than the primary peak due to a $\pi-\pi^*$ shakeup transition. The complex region around 291−292 eV makes peak fitting with a shakeup satellite very difficult, and therefore this weak shakeup feature was not included in the fitting. The lower binding energy peak at 284.3 eV is attributed to the aromatic carbons (in α and β positions) of e-PT.[33] There is no discernible lower energy shoulder below 283 eV, which should be the peak position for the metal−carbon bond.[34,35] Therefore, the aromatic carbon ring likely has no strong chemical bonding with Zn in the substrate. The atomic ratio of C:S is approximately 4.06:1, which is in agreement with the theoretical ratio of 4.00 for the monomer bithiophene used in electropolymerization. This indicates that the monomer largely maintains its molecular composition.

The electron inelastic mean free path (IMFP) of the Zn 2p photoelectron is ∼1 nm.[36] Hence, ∼95% of the Zn 2p photoemission intensity originates from the top 3 nm layer of the sample. The outermost monolayer of ZnO was reported to be ∼0.26 nm thick.[37] Assuming that the interfacial bonding occurs within this ZnO monolayer at 100% coverage (the active Zn sites should be much fewer in reality), the Zn available to bond to e-PT only represents a small fraction of the observable Zn and the majority of the Zn signal originates from the bulk ZnO film. In order to extract additional information for this study, the Zn $L_3M_{4,5}M_{4,5}$ Auger lines were analyzed. They are the Zn features that are most sensitive to changes in oxidation states, with a relatively big shift of ∼5 eV from Zn to ZnO, compared to a shift of only 0.1−0.2 eV in the Zn 2p XPS lines (Supporting Information, Figure S5).[38] The original spectrum of the Zn $L_3M_{4,5}M_{4,5}$ Auger peak is a broad feature with a shoulder (Supporting Information, Figure S6). Differentiation of the Auger spectrum can remove the background and enhance the features hidden in overlapping peaks. The first-derivative Zn $L_3M_{4,5}M_{4,5}$ Auger spectra of ZnO substrate (red line) and e-PT/ZnO (black line) are shown in Figure 1d.[39] Both spectra have two positive peaks at ∼991.7 eV and ∼988.7 eV and one negative peak at ∼986.3 eV. The positive peak at 991.7 eV represents the positive excursion of the differentiated Zn peak, while the negative peak at 986.3 eV comes from the negative excursion of the differentiated ZnO peak. Both of these peaks showed little change in intensity before and after electropolymerization. The positive peak at 988.7 eV in the ZnO substrate spectrum results from overlapping of the negative excursion of Zn and positive excursion of ZnO. This peak height has increased in the region with e-PT coverage compared to the substrate with no coverage. With the peak height of Zn and ZnO unchanged, the most probable scenario would be that there is a third component arising within this region which leads to the peak height increase. The peak separation between ZnS and Zn in the Auger spectrum is ∼3 eV.[40,41] With the Zn positive peak at 991.7 eV, the ZnS peak should appear at 988.7 eV if it exists. This kinetic energy coincides with the position where the peak intensity increases, implying that the third component is ZnS. Our S 2p XPS analysis (noted above), supported by these Zn LMM Auger results, suggests the existence of direct Zn−S bonding at the interface.

Thiophene can be oriented parallel to or upright from the ZnO surface via its aromatic carbon ring π electrons or the S lone pair of electrons, respectively. The change in thiophene bonding geometry from lying flat on the surface to standing upright from the surface (or any angle in between) is dependent on the coverage of the adsorbed thiophene.[18] Experimental and theoretical studies on sexithiophene (an oligomer that closely resembles short polymeric chains in e-PT) adsorption on TiO_2,[20] SiO_2,[21] and ZnO[22] all point to two predominant binding geometries as shown in Scheme 2: (i) standing up with its long axis normal to the surface and (ii) lying flat on the surface. One interesting observation about sexithiophene adsorption on SiO_2 demonstrated that, for submonolayer coverages, molecules standing up along their molecular axis coexist with those who are lying down on the substrate. When the first monolayer is completed, all sexithiophene molecules stand up on the surface and flat-lying molecules cannot be detected.[21] At low coverages, the flat-flying orientation is more energetically stable owing to a stronger orbital overlap between the thiophene π electrons and the substrate surface. For a monolayer or higher coverage, the total system energy (polymer−polymer intermolecular plus polymer−surface interactions) results in an upright orientation being favored.[22] This is likely analogous to our case with more than one monolayer coverage of e-PT on ZnO; therefore, the upright molecular orientation is expected. The S-end of the molecule and Zn forms chemical bonds, while the aromatic carbon ring has minimal interaction with the surface due to this specific geometry.

dx.doi.org/10.1021/jp400871g | J. Phys. Chem. C 2013, 117, 9852−9863

3.2.2. e-PT/ZnO Nanorod Substrates. In order to investigate the e-PT/ZnO nanorod interface, thin films of e-PT were electropolymerized onto ZnO nanorods at a low potential 0.95 V (barely over the 0.90 V minimal oxidation potential) for 77 s in a dilute 0.01 M monomer solution in dichloromethane.

The XPS wide energy scan is similar to the one observed for e-PT on ZnO films, thus it is omitted here. The S 2p spectrum (Figure 2a) shows a single doublet with the $2p_{3/2}$ peak centered

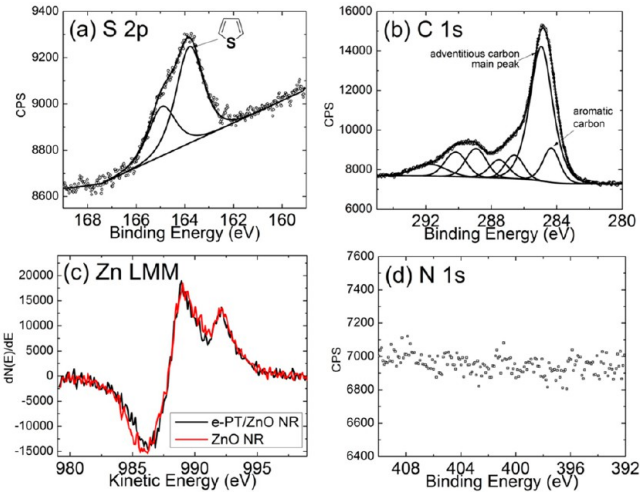

Figure 2. (a) S 2p and (b) C 1s XPS spectra of e-PT on ZnO nanorod substrate. (c) First-derivative spectra of Zn $L_3M_{4,5}M_{4,5}$ Auger spectrum of ZnO nanorod (NR) substrate with e-PT coverage (black line) and without e-PT coverage (red line). (d) N 1s XPS spectrum of ZnO nanorod substrate.

at 163.8 eV, which is in excellent agreement with our previous measurement of the S 2p binding energy at the interface of e-PT/ZnO films. There is no discernible ZnS shoulder in the S 2p spectrum of the e-PT/ZnO nanorod sample at lower binding energy, indicating a lack of chemical bonding between S and Zn. This is quite different from the e-PT/ZnO film interface, where a major peak was observed at 161.9 eV and attributed to Zn−S bonding.

In the C 1s spectrum (Figure 2b), the aromatic carbon peak shows up at the same binding energy as our above-noted results at 143.7 eV. There are four carbon peaks at higher binding energy (286.6, 287.5, 289.0, and 290.2 eV) analogous to the above-mentioned e-PT/ZnO film samples. A broad feature centered at 291.8 eV can be clearly modeled and is designated as the $\pi-\pi^*$ shakeup satellite. The lack of lower binding energy shoulder at around 281−282 eV demonstrates that a strong covalent interaction between aromatic C and Zn is not present.

The Zn $L_3M_{4,5}M_{4,5}$ first-derivative Auger spectrum (Figure 2c) shows virtually no intensity change for the three peaks (986.3, 988.9, and 992.0 eV) with or without e-PT coverage, further verification that there is no significant ZnS bonding at the interface. The kinetic energy of all three peaks is in agreement with the previous assignment on the e-PT/ZnO film.

The amine used during the hydrothermal synthesis, HMTA, may remain on the surface of the nanorods and interfere with the adsorption of e-PT onto ZnO nanorods. In one report, HMTA is suspected to adsorb on the nonpolar facets of ZnO nanorods and mediate their aspect ratio during hydrothermal growth.[42] However, such a hypothesis is contradicted by other studies that HTMA is likely to decompose rapidly at elevated temperatures during the synthesis to yield formaldehyde and ammonia.[43,44] Even if there is amine present on the sidewalls of the as-grown nanorods, the adsorption is weak enough that rinsing with water should eliminate its presence, as is evidenced in a report about ethyelenediamine adsorption on ZnO nanorods.[45] In order to confirm that no HMTA adsorption on ZnO nanorods survives rinsing with water, a N 1s XPS scan (Figure 2d) was performed and revealed no detectable peak intensity. This points to the lack of HMTA adhesion to the nonpolar facets of ZnO nanorods after rinsing with water; hence, we rule out the possibility of HMTA interference with the adsorption of e-PT on ZnO nanorods. In summary, there is no indication of sulfide or carbide bonding of e-PT on ZnO nanorods from XPS and Auger analyses. In addition, there is no HMTA present on the nanorods to interfere with our interpretation.

3.2.3. Polarity and Defects of ZnO Surfaces. Our XPS results show that the as-deposited e-PT interacts strongly with the ZnO planar substrate. It is chemisorbed to the ZnO substrate via sulfur in the thiophene unit. The carbon ring, by contrast, does not appear to have significant direct bonding with the ZnO substrate. By contrast, e-PT does not bond strongly with the ZnO nanorod surface, and their interaction is probably limited to physisorption (e-PT films can still be grown conformally along the ZnO nanorods; see also Section 3.3).

ZnO exhibits strongly anisotropic morphology with a variety of polar and nonpolar surfaces. ZnO planar substrates were found to be *c*-axis aligned with a polar (0001) surface.[46] ZnO nanorods, on the other hand, are mostly comprised of sidewalls that are nonpolar mixed-terminated $(10\bar{1}0)$ surfaces. Both theoretical calculations and experimental results suggest the nonpolar $(10\bar{1}0)$ surface as the most stable face; hence it can be expected to have a lower adsorption strength relative to the polar Zn-(0001) face.[47] Adsorption studies of various alcohol molecules on single crystal ZnO surfaces also demonstrate the Zn-(0001) face is the most strongly adsorbed.[48] Selective adsorption of certain moieties on polar and nonpolar surface was recently reported, with citric acid selectively adsorbing on ZnO polar surfaces and ethylenediamine on ZnO nonpolar surfaces.[45] Alkylthiols were found to adsorb on ZnO films[14,16,17] which have polar surfaces, but not on MOCVD-grown ZnO nanorods which consist mostly of nonpolar surfaces.[15] We believe the different bonding nature of e-PT to ZnO film and nanorod substrates that we observe is similarly influenced by the different polarity of ZnO surfaces.

The surface chemistry of ZnO can be rather complex. One should consider that surface defect chemistry may also play an important role in mediating the interaction between e-PT and ZnO. Surface defects on ZnO crystals are dominated by oxygen vacancies (V_O).[49] To this end, XPS can be used to quantify the amount of V_O by careful studies of the O 1s and Zn 2p spectra. For ZnO films with e-PT adsorbed, the O 1s peak (Figure 3a) can be fit with two peaks centered at 530.4 and 531.9 eV. For e-PT covered ZnO nanorods, the O 1s peak (Figure 3b) can be fit with three peaks at 530.0, 531.8, and 533.4 eV. The low binding energy component at 530.2 ± 0.2 eV (denoted as O_A), is attributed to the O^{2-} ions in the normal wurtzite structure of ZnO.[50] The medium binding energy component at 531.8−531.9 eV (denoted as O_B), has been assigned to two different contributions in the literature: O^{2-} ions in oxygen deficient regions of ZnO,[51] or adsorbed OH groups on the surface (Scheme 3).[52] Further analysis is needed to delineate the real contribution of O_B. We use the O 1s spectrum of e-PT/ZnO

dx.doi.org/10.1021/jp400871g | J. Phys. Chem. C 2013, 117, 9852−9863

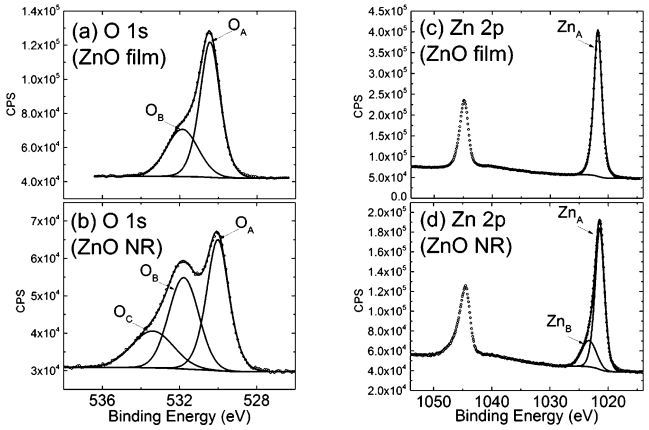

Figure 3. O 1s XPS spectra of e-PT covered (a) ZnO film and (b) ZnO nanorod; Zn 2p XPS spectra of e-PT covered (c) ZnO film and (d) ZnO nanorod.

Scheme 3. Surface Structure Model of (0001) Plane ZnO with Oxygen Vacancies and OH Groups

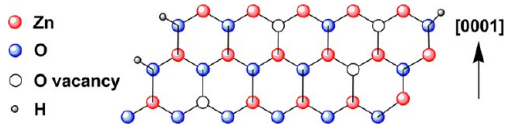

films as an example. If O_B is solely assigned to O^{2-} ions in oxygen deficient regions, then the total oxygen to Zn ratio (O_A + O_B):Zn would be 0.96, which indicates that there are only 4% oxygen vacancies and that ZnO is nearly stoichiometric. This calculation contradicts the observation that there is a prominent O_B component which implies a significant oxygen deficiency (~34% of the total oxygen content at the surface). Therefore, a reasonable explanation is that O_B is the combination of two inseparable peaks of both O^{2-} ions in oxygen deficient regions and OH groups on the surface. The high binding energy O_C peak, which only appears on the ZnO nanorod sample at 533.4 eV, is attributed to loosely bound oxygen species such as H_2O on the ZnO surface.[52] Interestingly, there appears to be an additional Zn $2p_{3/2}$ peak for ZnO nanorod samples: the higher binding energy edge of Zn $2p_{3/2}$ peak is less sharp in the nanorod sample (Figure 3b) than in film sample (Figure 3a), and this peak must be fit with two components Zn_A and Zn_B at 1021.5 and 1023.3 eV, respectively. We think that Zn_B represents the Zn species bound to oxygen species such as H_2O, similar to the origin of O_C component. The appearance of O_C and Zn_B only in ZnO nanorods probably stems from the specific synthetic routes. The sol–gel ZnO film was synthesized with thermal annealing in air. The hydrothermal synthesis of ZnO nanorods, on the other hand, was performed in an aqueous solution.[52,53]

Due to the overlap of the two contributions to the O_B peak which complicates quantification, O_A (normal wurtzite structure) is used to determine the oxygen deficiency in ZnO films and nanorods. The ratio of O_A/Zn is 0.63 and 0.54 for the ZnO film and nanorods, respectively. This indicates that the ZnO film surface has fewer defects (V_O) than the nanorod surface. Studies have shown that the introduction of V_O will reduce the positive charge of the adjacent Zn^{2+} species and increase its probability to chemisorb molecules.[18,54] If the surface defects played a significant role, the ZnO film surface should have exhibited less chemisorption than ZnO nanorods. However, this is not the case; thus we believe that surface defects are not significant in determining the adsorption behavior of e-PT on ZnO.

To summarize, the different adsorption behavior of e-PT on ZnO planar and nanorod substrates is mainly attributed to different polarity of ZnO surfaces while the influence of surface defects was found to be minor.

3.3. Morphological Control. *3.3.1. Film Thickness Monitored by Electrochemical Charge.* The e-PT film thickness can be regulated by the total electrochemical charge used during electropolymerization. In an ideal situation, the charge applied to the electrochemical system will be completely used to electro-oxidize the monomers and oligomers in the solution to form polymeric layers on the ZnO surface. In reality, the polymerization of each bithiophene monomer unit involves the removal of about 2.25 electrons.[55] Therefore, the film thickness d can be estimated by the total charge in the monomer oxidation process, Q, using the following equation: $[Q/2.25eN_0]M_w = \rho Sd$, where e is the electron charge, N_0 is Avogadro's constant, M_w is the molecular weight of bithiophene (166 g/mol), S is the area of the film (~1 cm^2), and ρ is the density of the film and assumed to be 1.5 g/cm^3.[56] This equation implies a direct proportional relationship between the total charge and the film thickness. In an actual setting, there is always a relatively small portion of the charge that is used to form oligomeric species that are soluble in the electrochemical solution yet do not attach to the surface. Nonetheless, qualitatively speaking, the electrochemical charge remains an effective real-time monitor for film thickness during electropolymerization. It is automatically calculated by integrating the area under the I–t curve with the progression of time on our

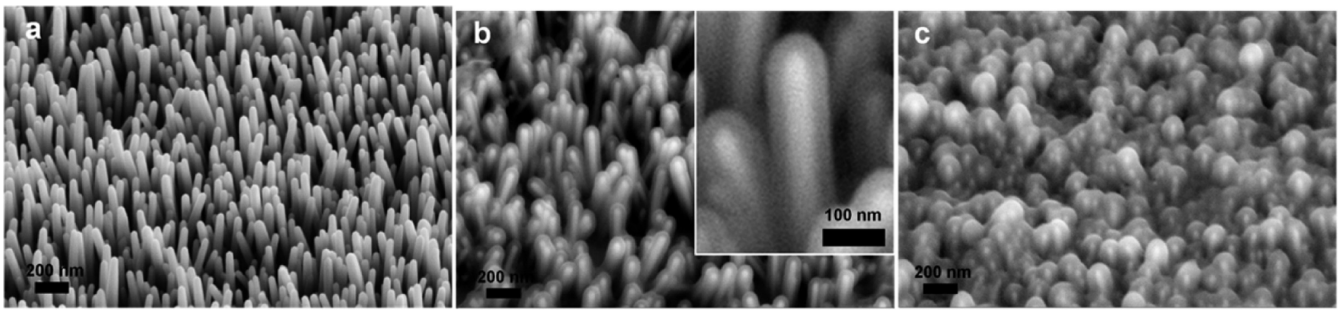

Figure 4. SEM images (45° tilt angle) of (a) ZnO nanorods before electropolymerization, (b) e-PT/ZnO nanorods at an electrochemical charge of 4 mC, and (c) e-PT/ZnO nanorods at a polymerization charge of 9 mC. Inset in part b shows the magnified view of e-PT/ZnO nanorods. The solvent used in electropolymerization is dichloromethane.

dx.doi.org/10.1021/jp400871g | J. Phys. Chem. C 2013, 117, 9852–9863

Figure 5. Cross-sectional SEM images of e-PT on ZnO nanorods at an electrochemical charge of (a) 8, (b) 25, and (c) 75 mC. The solvent used in electropolymerization is acetonitrile.

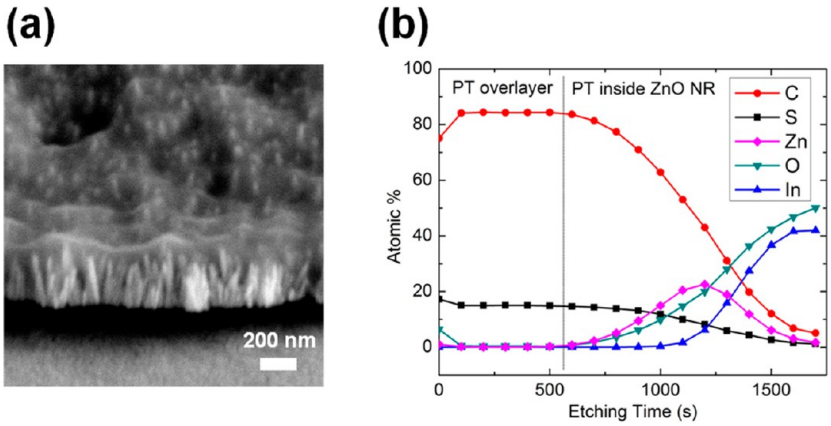

Figure 6. (A) SEM image (taken at 45° tilt angle) of e-PT on ZnO nanorods after thermal annealing. (B) Plot of atomic percentage and etching time for various elements in XPS depth profiling experiment.

instrument (charge is noted in units of millicoulomb, mC). In the following sections, we vary the electrochemical charge to study the evolution of film morphology in two solvents, DCM and ACN.

3.3.2. Electropolymerization in Dichloromethane: Core–Shell Structure. Electropolymerization of PT on ZnO nanorods in DCM was investigated by SEM. Figure 4a shows the ZnO nanorod morphology before electropolymerization. After a small charge of ~4 mC was delivered to the electrochemical cell, we observe a core–shell structure with a polymer layer of ~30 nm electrodeposited along the ZnO nanorods (Figure 4b). The e-PT film is highly conformal and smooth, and there is excellent contact and wetting between e-PT and ZnO. This morphology is particularly encouraging for PV and related applications as the interfacial surface area is maximized relative to what we observe by spin coating or drop casting. After the polymerization charge is increased to 9 mC, a thicker e-PT shell of ~60 nm was produced over the nanorods (Figure 4c). The thicker e-PT film fully coats the area between the rods with polymer and adopts a ripple-like morphology over the tips of the nanorods. These morphology observations indicate that the polymer growth expands radially on the nanorods and converges between adjacent nanorods at a longer growth time, leaving only the nanorod tips visible to our SEM observation.

3.3.3. Electropolymerization in Acetonitrile: Bulk Heterojunction Structure. Polymer films of increasing thickness were deposited in ACN as the electrochemical charge was varied from 8 to 75 mC. The film morphology in ACN was markedly different than that in DCM. At 8 mC, the charge dispensed through the electrochemical cell afforded a thin polymeric film along the ZnO nanorods, though the film growth appears less conformal and more nodular than that in DCM (Figure 5a). After a charge of 25 mC was consumed, the polymer forms a thicker overlayer of ~50 nm with substantial roughness on top of the nanorods (Figure 5b). For a higher charge of 75 mC, the polymer overlayer grew to ~200 nm (Figure 5c). At higher electrochemical charges such as 25 or 75 mC, bulk heterojunction (BHJ) structures of interdigitated polymer and ZnO nanorods with a polymer overlayer on top of the nanorods were produced. The polymer overlayer may function as an electron blocking layer and increase the device performance.[57] Therefore, these BHJ structures were used to fabricate solar cells (see Section 4 for more details about device testing).

3.3.4. Solvent Polarity. The polarity of the solvent molecule is a key factor determining film morphology. The higher polarity solvent (ACN) is considered to interact more strongly with the surface than the less polar solvent (DCM), competing with monomer/oligomer adsorption on the surface and in effect reducing the density of polymer nucleation sites.[30] This results in more conformal and intimate contact with the nanorods in DCM than in ACN. The morphologically rougher polymeric overlayer formed in ACN than in DCM may be due to the different solubilities of oligomers in the two solvents.[58] Oligomers are less soluble in ACN than in DCM, thus supersaturation above the electrode is more rapidly attained in ACN, enabling polymeric clusters to deposit onto the electrode and create growing nuclei that promote three-dimensional growth.[59] To summarize, core–shell and BHJ structures can be

dx.doi.org/10.1021/jp400871g | J. Phys. Chem. C 2013, 117, 9852–9863

obtained by altering the solvent used in electropolymerization. Our results demonstrate the surface-initiating nature of electropolymerization and contribute to further understanding of electropolymerization growth kinetics in different solvents.

3.3.5. Complete Polymer Infiltration: XPS Depth Profiling. The polymer filling in a BHJ structure can be further improved by thermal annealing. An e-PT/ZnO nanorods/ITO sample was electrodeposited potentiodynamically (−0.5 to 1.4 V, 2 cycles, 100 mV/s, in ACN), followed by thermal annealing at 300 °C for 30 min in argon. From the SEM image (Figure 6a), it is difficult to accurately observe the depth and completeness of polymer infiltration. XPS depth profiling with Ar^+ sputtering (Figure 6b) was used as a supplemental technique to probe if the polymer fully infiltrated the nanorods. The sputtering depth is related to the etch time. The most intense and the most suitable XPS peak of each element (C 1s, S 2p, Zn 2p, O 1s, and In 3d) was used to determine the atomic percentage at any given etch time. Before the etching time of 500 s, the sputtered material consists solely of the polymer overlayer on top of the nanorods as only C and S signals are observed. Then the C and S signals from e-PT gradually decrease as the sputtering penetrates the e-PT/ZnO nanorod network. Meanwhile, the Zn and O photoemission intensities from the ZnO nanorods slowly increase. At 1000 s, In (from the ITO substrate beneath the ZnO film) appears in the elemental composition, indicating that the ITO film has been exposed to sputtering. The bombardment of Ar^+ on surfaces not covered by the nanorods should occur earlier than those covered with the nanorods. This results in an overlap of In and Zn signal from 1000 s. The C and S signals, with their ratio constant at ~4:1 throughout the etching, coexist with the Zn signal until Zn is completely depleted at 1700 s. This suggests that e-PT has infiltrated to the bottom of the dense ZnO nanorod arrays, which leads to higher interfacial area beneficial for PV applications.

4. RELATIONSHIP BETWEEN DEVICE PERFORMANCE AND POLYMER STRUCTURE

Photovoltaic *J*−*V* device testing (Figure 7, Table 1) was performed on e-PT/ZnO bilayer and nanorod structures, with and without a hole injection layer, PEDOT:PSS. We again note that unsubstituted PT without side chains is not an ideal polymer for a high efficiency solar cell. It is, however, a simple model system that we use to develop a more comprehensive understanding of bonding, structure, and optoelectronic response, all key components of a polymer solar cell.

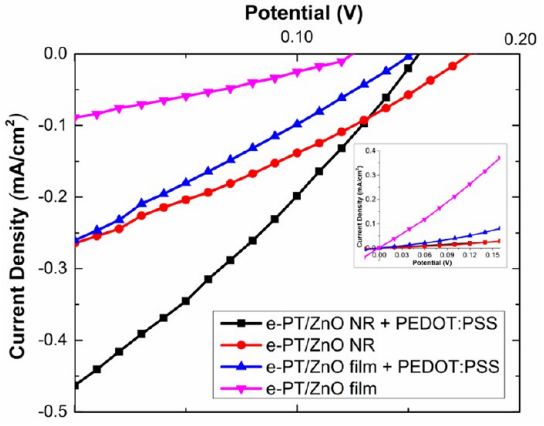

Figure 7. *J*−*V* characterization of e-PT solar cells. Inset shows dark *J*−*V* curves.

Table 1. Photovoltaic Parameters

sample	PEDOT:PSS	J_{SC} (mA/cm^2)	V_{OC} (V)	FF	PCE (%)
e-PT/ZnO film	no	0.089	0.13	0.29	0.003
e-PT/ZnO film	yes	0.260	0.16	0.25	0.011
e-PT/ZnO nanorods	no	0.264	0.18	0.29	0.014
e-PT/ZnO nanorods	yes	0.463	0.16	0.28	0.021

All e-PT samples were electropolymerized in ACN at a fixed polymerization charge of 75 mC which produces BHJ structures with a thick polymer overlayer (~150 nm) on top of the ZnO nanorods. This overlayer acts as an electron blocking layer and prevents nanorods "poking through" the polymer and shorting the device. The BHJ solar cells performed significantly better than the planar bilayer structures. This improvement, which shows up as a higher J_{SC}, occurs mainly because the ZnO nanorods improve the surface area of the organic−inorganic interface, enabling more charge separation and less recombination.[60] The conduction bands of the ZnO film and nanorods are expected to be similar, therefore there should be little variation in V_{OC} between the bilayer and nanostructure active layers. The function of the hole injection layer, PEDOT:PSS, is to block the electrons from reaching the Ag electrode and thus reduce the leakage current and increase J_{SC} without sacrificing V_{OC} or FF. The efficiencies for devices with PEDOT:PSS are higher than those without such a layer due to a higher J_{SC}, as expected. BHJ device with PEDOT:PSS and a Ag electrode are shown in Figure 8.

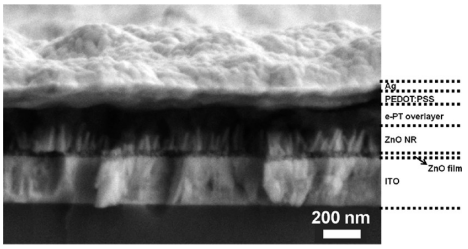

Figure 8. Cross-sectional SEM image of a typical e-PT/ZnO nanorod device.

The relatively low fill factor (FF) values are most likely due to low carrier mobilities and hence high bimolecular recombination rates.[61] The e-PT film generally has carrier mobilities orders of magnitude lower than those of commercially available regioregular-P3HT.[9] P3HT has relatively narrow polydispersity and low impurity concentrations (which comes from rigorous purification). Electropolymerization can produce regiorandom polymers with structural defects of undesirable α−β linkages and cross-linking between adjacent chains. This results in a disruption to the conjugation length, poor chain packing, low crystallinity, and low carrier mobilities. This is especially severe for thicker films, as the accumulation of structural defects increasingly degrades the electronic properties of the polymer.[62,63] Our UPS He I results (Supporting Information, Table S1) showed a small downshifting of the HOMO levels of e-PT films as the film thickness increases, which has recently been correlated with increasingly regiorandom polymeric structures in the literature.[64] Therefore, UPS

dx.doi.org/10.1021/jp400871g | J. Phys. Chem. C 2013, 117, 9852−9863

results corroborate with observations of other researchers that thicker electropolymerized films accumulate more structural defects and subsequently yield poor electronic properties such as lower carrier mobility.[52−54]

The growth of electropolymerized polymers on surfaces can be generally considered as the formation of a two-dimensional (2D) film followed by three-dimensional (3D) nodular growth.[30,59] We also observe that thicker electropolymerized films display a nodular surface with cracks (Supporting Information, Figure S7). Partial shorting of devices by exposed ZnO nanorods coming into close or direct contact with the Ag electrode leads to higher leakage currents and lower J_{SC}. Growing thicker polymer films does not appear to significantly decrease device leakage or improve performance as roughening and stress-related cracking become more pronounced.

V_{OC} and FF are often interconnected and a lower FF can lead to a lower V_{OC} value.[65] The theoretical maximum V_{OC} is determined by the difference between the HOMO level of e-PT and the conduction band of ZnO nanorods, provided that there are ohmic contacts at both electrodes. At close proximity to the organic−inorganic interface, represented by sample A and B, the HOMO levels of e-PT is 4.7−4.8 eV. It was reported that ZnO nanorods have a conduction and valence band of ∼4.0 eV and ∼7.5 eV, respectively.[66] We can then estimate the theoretical maximum V_{OC} for e-PT/ZnO nanorods to be 0.7−0.8 V, which is close to the highest reported V_{OC} (0.63 V) for P3HT/ZnO nanorods devices.[67]

On the basis of the above discussion, thinner polymer films that are more crystalline and compact will translate to higher carrier mobilities and fewer structural defects, resulting in better performing devices. The initial intention of growing a thick polymer overlayer (shown in Figure 8) originated from studies on P3HT/ZnO nanorods, in which the authors found that a polymer overlayer of a certain thickness (∼250 nm) functions as an electron-blocking layer and improves the device efficiency.[57] However, the e-PT overlayer has a much lower mobility than P3HT. It may still function as an electron blocking layer, but overall thick films are detrimental to the device performance.

PV devices fabricated from electropolymerized polymers on high aspect ratio nanostructures, usually consist of a thin polymer layer grown along the nanorods instead of a thick polymer overlayer grown above the nanorod arrays as is in our devices.[9−13] The developing consensus in the literature, supported by our results, is that thin layers of electropolymerized polymer grown along the nanostructure surface, circumvents the inherent problem with electropolymerization for thicker polymeric layers and preserves the surface-initiating advantage of such a polymerization method to achieve high filling rates in the dense nanorod arrays.

5. CONCLUSIONS

We used an electropolymerization method to improve the filling of a polymer inside a high density nanorod array. Enhancing the polymer filling fraction may be advantageous for hybrid solar cell and other applications because it produces a high surface area for charge separation.

Interfacial bonding between e-PT films and ZnO planar/nanorod substrates was investigated by XPS. We found that the e-PT films were chemisorbed onto ZnO planar substrates primarily via Zn−S bonding and likely adopt an upright molecular geometry on the surface. By contrast, there was no strong covalent bonding detected for e-PT films adsorbed on ZnO nanorod substrates. The different bonding nature of e-PT films to the two surfaces is mainly attributed to the different surface polarities: ZnO planar substrates have a polar Zn-(0001) surface, whereas ZnO nanorods have mostly nonpolar $(10\bar{1}0)$ sidewalls. Point defects, predominantly oxygen vacancies in ZnO, were found to have a relatively insignificant influence on the adsorption behavior of e-PT films on ZnO surfaces.

The solvent used in electropolymerization was found to affect the final morphology of the e-PT films on ZnO nanorods. Highly conformal growth along the nanorods with intimate contact between the two phases was observed in e-PT films electrodeposited in DCM. When the solvent is changed to ACN, the film growth becomes less conformal and more nodular around the nanorods. The film morphological control was attained by changing the polarity of the solvent, with ACN being the more polar molecule and likely competing with the monomer for adsorption on the electrode and hence reducing monomer coverage.

Device testing on e-PT/ZnO hybrid solar cells yielded low power conversion efficiencies, presumably due to the known lower carrier mobility of regiorandom e-PT compared to regioregular polymers such as P3HT. Within the e-PT system, we found that thicker films have a higher degree of structural irregularity which translates to a further decrease in carrier mobility and device performance. Our findings suggest that a core−shell structure with a thin e-PT film along the nanorods will produce better performing devices and is the subject of our ongoing studies.

■ ASSOCIATED CONTENT

Ⓢ Supporting Information

XRD graph of ZnO nanorods (Figure S1). Normalized UV−vis absorption and PL spectra (Figure S2). UPS He II spectrum (Figure S3). S 2p XPS spectrum of a bulk PBT film (Figure S4). Zn 2p XPS spectrum and Zn $L_3M_{4,5}M_{4,5}$ Auger spectrum of ZnO planar substrates with and without e-PT coverage (Figures S5 and S6). SEM image of a morphological defect in thicker e-PT film (Figure S7). Summary of UPS He I results (Table S1). This material is available free of charge via the Internet at http://pubs.acs.org.

■ AUTHOR INFORMATION

Corresponding Author

* Phone: 732-445-2747. E-mail: egarf@rutgers.edu.

Notes

The authors declare no competing financial interest.

■ ACKNOWLEDGMENTS

National Science Foundation (DMR 1006740) financial support for this work is gratefully acknowledged. The authors also acknowledge Dr. Tom Emge for XRD collection and Dr. Xinsheng Liu and Dr. Shouhua Feng for helpful discussion.

■ REFERENCES

(1) Li, G.; Zhu, R.; Yang, Y. Polymer Solar Cells. *Nat. Photonics* **2012**, *6*, 153−161.

(2) Gunes, S.; Neugebauer, H.; Sariciftci, N. S. Conjugated Polymer-based Organic Solar Cells. *Chem. Rev.* **2007**, *107*, 1324−1338.

(3) Li, Y. Molecular Design of Photovoltaic Materials for Polymer Solar Cells: Toward Suitable Electronic Energy Levels and Broad Absorption. *Acc. Chem. Res.* **2012**, *45*, 723−733.

(4) Shaw, P. E.; Ruseckas, A.; Samuel, I. D. W. Exciton Diffusion Measurements in Poly(3-hexylthiophene). *Adv. Mater.* **2008**, *20*.
(5) Boucle, J.; Ravirajan, P.; Nelson, J. Hybrid Polymer−Metal Oxide Thin Films for Photovoltaic Applications. *J. Mater. Chem.* **2007**, *17*, 3141−3153.
(6) Lee, Y.-J.; Lloyd, M. T.; Olson, D. C.; Grubbs, R. K.; Lu, P.; Davis, R. J.; Voigt, J. A.; Hsu, J. W. P. Optimization of ZnO Nanorod Array Morphology for Hybrid Photovoltaic Devices. *J. Phys. Chem. C* **2009**, *113*, 15778−15782.
(7) Bartholomew, G. P.; Heeger, A. J. Infiltration of Regioregular Poly[2,2′-(3-hexylthiopene)] into Random Nanocrystalline TiO_2 Networks. *Adv. Funct. Mater.* **2005**, *15*, 677−682.
(8) Briseno, A. L.; Holcombe, T. W.; Boukai, A. I.; Garnett, E. C.; Shelton, S. W.; Frechet, J. J. M.; Yang, P. Oligo- and Polythiophene/ZnO Hybrid Nanowire Solar Cells. *Nano Lett.* **2010**, *10*, 334−340.
(9) Xi, D.; Zhang, H.; Furst, S.; Chen, B.; Pei, Q. Electrochemical Synthesis and Photovoltaic Property of Cadmium Sulfide-Polybithiophene Interdigitated Nanohybrid Thin Films. *J. Phys. Chem. C* **2008**, *112*, 19765−19769.
(10) Sun, B.; Hao, Y.; Guo, F.; Cao, Y.; Zhang, Y.; Li, Y.; Xu, D. Fabrication of Poly(3-hexylthiophene)/CdS/ZnO Core-shell Nanotube Array for Semiconductor-sensitized Solar Cell. *J. Phys. Chem. C* **2011**, *116*, 1395−1400.
(11) Dobbelin, M.; Tena-Zaera, R.; Carrasco, P. M.; Sarasua, J.-R.; Cabanero, G.; Mecerreyes, D. Electrochemical Synthesis of Poly(3,4-ethylenedioxythiophene) Nanotube Arrays Using ZnO Templates. *J. Polym. Sci., Part A: Polym. Chem.* **2010**, *48*, 4648−4653.
(12) Mariani, G.; Laghumavarapu, R. B.; Villers, B. T. d.; Shapiro, J.; Senanayake, P.; Lin, A.; Schwartz, B. J.; Huffaker, D. L. Hybrid Conjugated Polymer Solar Cells Using Patterned GaAs Nanopillars. *Appl. Phys. Lett.* **2010**, *97*, 013107.
(13) Giacomo, M.; Wang, Y.; Wong, P.-S.; Lech, A.; Hung, C.-H.; Shapiro, J.; Prikhodko, S.; El-Kady, M.; Kaner, R. B.; Huffaker, D. L. Three-Dimensional Core-Shell Hybrid Solar Cells via Controlled in Situ Materials Engineering. *Nano Lett.* **2012**, *12*, 3581−3586.
(14) Ogata, K.; Hama, T.; Hama, K.; Koike, K.; Sasa, S.; Inoue, M.; Yano, M. Characterization of Alkanethiol/ZnO Structures by X-ray Photoelectron Spectroscopy. *Appl. Surf. Sci.* **2005**, *241*, 146−149.
(15) Taratula, O.; Galoppini, E.; Wang, D.; Chu, D.; Zhang, Z.; Chen, H.; Saraf, G.; Lu, Y. Binding Studies of Molecular Linkers to ZnO and MgZnO Nanotip Films. *J. Phys. Chem. B* **2006**, *110*, 6506−6515.
(16) Sadik, P. W.; Pearton, S. J.; Norton, D. P.; Lambers, E.; Ren, F. Functionalizing Zn- and O-terminated ZnO with Thiols. *J. Appl. Phys.* **2007**, *101*, 104514.
(17) Perkins, C. L. Molecular Anchors for Self-assembled Monolayers on ZnO: A Direct Comparison of the Thiol and Phosphonic Acid Moieties. *J. Phys. Chem. C* **2009**, *113*, 18276−18286.
(18) Liu, G.; Rodriguez, J. A.; Hrbek, J.; Long, B. T.; Chen, D. A. Interaction of Thiophene with Stoichiometric and Reduced Rutile TiO_2(110) Surfaces: Role of Ti_3^+ Sites in Desulfurization Activity. *J. Mol. Catal. A: Chem.* **2003**, *202*, 215−227.
(19) Jirsak, T.; Dvorak, J.; Rodriguez, J. A. Chemistry of Thiophene on ZnO, S/ZnO, and Cs/ZnO Surfaces: Effects of Cesium on Desulfurization Processes. *J. Phys. Chem. B* **1999**, *103*, 5550−5559.
(20) Ivanco, J.; Haber, T.; Krenn, J. R.; Netzer, F. P.; Resel, R.; Ramsey, M. G. Sexithiophene Films on Ordered and Disordered TiO_2(110) Surfaces: Electronic, Structural and Morphological Properties. *Surf. Sci.* **2007**, *601*, 178−187.
(21) Loi, M. A.; Como, E. D.; Dinelli, F.; Murgia, M.; Zamboni, R.; Biscarini, F.; Muccini, M. Supramolecular Organization in Ultra-thin Films of α-Sexithiophene on Silicon Dioxide. *Nat. Mater.* **2005**, *4*, 81−85.
(22) Sai, N.; Leung, K.; Chelikowsky, J. R. Hybrid Density Functional Study of Oligothiophene/ZnO Interface for Photovoltaics. *Phys. Rev. B* **2011**, *83*, 121309.
(23) Yamabi, S.; Imai, H. Growth Conditions for Wurtzite Zinc Oxide Films in Aqueous Solution. *J. Mater. Chem.* **2002**, *12*, 3773−3778.
(24) Greene, L. E.; Law, M.; Tan, D. H.; Montano, M.; Goldberger, J.; Somorjai, G.; Yang, P. General Route to Vertical ZnO Nanowire Arrays Using Textured ZnO Seeds. *Nano Lett.* **2005**, *5*.
(25) Gonzalez-Moreno, R.; Cook, P. L.; Zegkinoglou, I.; Liu, X.; Johnson, P. S.; Yang, W.; Ruther, R. E.; Hamers, R. J.; Tena-Zaera, R.; Himpsel, F. J.; et al. Attachment of Protoporphyrin Dyes to Nanostructured ZnO Surfaces: Characterization by Near Edge X-ray Absorption Fine Structure Spectroscopy. *J. Phys. Chem. C* **2011**, *115*, 18195−18201.
(26) Funt, B. L.; Lowen, S. V. Mechanistic Studies of the Electropolymerization of 2,2′-Bithiophene and of Pyrrole to Form Conducting Polymers. *Synth. Met.* **1985**, *11*, 129−137.
(27) Waltman, R. J.; Bargon, J.; Diaz, A. F. Electrochemical Studies of Some Conducting Polythiophene Films. *J. Phys. Chem.* **1983**, *87*, 1459−1463.
(28) Sato, T.; Fujistsuka, M.; Segawa, H.; Shimidzu, T.; Tanaka, S. Dual Photoluminescence of Polythiophene Thin Films. *Synth. Met.* **1998**, *95*, 107−112.
(29) Wu, C.; Nilsson, J.; Inganas, O.; Salaneck, W.; Osterholm, J. E.; Bredas, J. Electronic Structure of Polythiophene. *Synth. Met.* **1987**, *21*, 197−202.
(30) del Valle, M. A.; Cury, P.; Schrebler, R. Solvent Effect on the Nucleation and Growth Mechanisms of Poly(thiophene). *Electrochim. Acta* **2002**, *48*, 397−405.
(31) Barreca, D.; Tondello, E.; Lydon, D.; Spalding, T. R.; Fabrizio, M. Single-Source CVD of Zinc Sulfide-based Thin Films from Zinc bis(*O*-ethylxanthate). *Chem. Vap. Deposition* **2003**, *9*, 93−98.
(32) Heeg, J.; Kramer, C.; Wolter, M.; Michaelis, S.; Plieth, W.; Fischer, W.-J. Polythiophene - O_3 Surface Reactions Studied by XPS. *Appl. Surf. Sci.* **2001**, *180*, 36−41.
(33) Morea, G.; Sabbatini, L.; Zambonin, P. G.; Swift, A. J.; West, R. H.; Vickerman, J. C. Modification of Polybithiophene by Electrochemical Cycling Studied by ToF-SIMS and XPS. *Macromolecules* **1991**, *24*, 3630−3637.
(34) Dannetun, P.; Boman, M.; Stafstrom, S.; Salaneck, W. R.; Lazzaroni, R.; Fredriksson, C.; Bredas, J. L.; Zamboni, R.; Taliani, C. The Chemical and Electronic Structure of the Interface between Aluminum and Polythiophene Semiconductors. *J. Chem. Phys.* **1993**, *99*, 664−672.
(35) Demirkan, K.; Mathew, A.; Weiland, C.; Reid, M.; Opila, R. L. Reactivity and Morphology of Vapor-Deposited Al/Polymer Interfaces for Organic Semiconductor Devices. *J. Appl. Phys.* **2008**, *103*, 034505.
(36) Tanuma, S.; Shiratori, T.; Kimura, T.; Goto, K.; Ichimura, S.; Powell, C. J. Experimental Determination of Electron Inelastic Mean Free Paths in 13 Elemental Solids in the 50 to 5000 eV Energy Range by Elastic-Peak Electron Spectroscopy. *Surf. Interface Anal.* **2005**, *37*, 833−845.
(37) Dulub, O.; Diebold, U.; Kresse, G. Novel Stabilization Mechanism on Polar Surfaces: ZnO(0001)-Zn. *Phys. Rev. Lett.* **2003**, *90*, 016102.
(38) Martin-Concepcion, A. I.; Yubero, F.; Espinos, J. P.; Gonzalez-Elipe, A. R.; Tougaard, S. X-ray Photoelectron Spectroscopy Study of the First Stages of ZnO Growth and Nanostructure Dependence of the Effects of Polarization at ZnO/SiO_2 and ZnO/Al_2O_3 Interfaces. *J. Vac. Sci. Technol., A* **2003**, *21*, 1393−1398.
(39) Briggs, D.; Seah, M. P. *Practical Surface Analysis*, 2nd ed.; John Wiley & Sons: West Sussex, 1990; Vol. *1*.
(40) Deroubaix, G.; Marcus, P. X-ray Photoelectron Spectroscopy Analysis of Copper and Zinc Oxides and Sulphides. *Surf. Interface Anal.* **1992**, *18*, 39−46.
(41) Critchley, B. R.; Stevens, P. R. C. Composition of RF-sputtered ZnS films. *J. Phys. D: Appl. Phys.* **1978**, *11*, 491−498.
(42) Sugunan, A.; Warad, H. C.; Boman, M.; Dutta, J. Zinc Oxide Nanowires in Chemical Bath on Seeded Substrates: Role of Hexamine. *J. Sol-Gel Sci. Technol.* **2006**, *39*, 49−56.
(43) Xu, S.; Lao, C.; Weintraub, B.; Wang, Z. L. Density-Controlled Growth of Aligned ZnO Nanowire Arrays by Seedless Chemical Approach on Smooth Surfaces. *J. Mater. Res.* **2008**, *23*, 2072−2077.

(44) Lee, Y.; Zhang, Y.; Ng, S. L. G.; Kartawidjaja, F. C.; Wang, J. Hydrothermal Growth of Vertical ZnO Nanorods. *J. Am. Ceram. Soc.* **2009**, *92*, 1940−1945.
(45) Nicholas, N. J.; Franks, G. V.; Ducker, W. A. Selective Adsorption to Particular Crystal Faces of ZnO. *Langmuir* **2012**, *28*, 7189−7196.
(46) Claeyssens, F.; Freeman, C. L.; Allan, N. L.; Sun, Y.; Ashfold, M. N. R.; Harding, J. H. Growth of ZnO Thin Films - Experiment and Theory. *J. Mater. Chem.* **2005**, *15*, 139−148.
(47) Dulub, O.; Boatner, L. A.; Diebold, U. STM Study of the Geometric and Electronic Structure of ZnO (0001)-Zn, (000-1)-O, (10-10), and (11-20) Surfaces. *Surf. Sci.* **2002**, *519*, 201−217.
(48) Henrich, V. E.; Cox, P. A. *The Surface Science of Metal Oxides*; Cambridge University Press: Cambridge, 1994.
(49) Lany, S.; Zunger, A. Dopability, Intrinsic Conductivity, and Nonstoichiometry of Transparent Conducting Oxides. *Phys. Rev. Lett.* **2007**, *98*, 045501.
(50) Coppa, B. J.; Davis, R. F.; Nemanich, R. J. Gold Schottky Contacts on Oxygen Plasma-Treated, n-Type ZnO (0001). *Appl. Phys. Lett.* **2003**, *82*, 400−402.
(51) Fan, J. C. C.; Goodenough, J. B. X-ray Photoemission Spectroscopy Studies of Sn-Doped Indium Oxide Films. *J. Appl. Phys.* **1977**, *48*, 3524−3531.
(52) Ogata, K.; Komuro, T.; Hama, K.; Koike, K.; Sasa, S.; Inoue, M.; Yano, M. Control of Chemical Bonding of the ZnO Surface Grown by Molecular Beam Epitaxy. *Appl. Surf. Sci.* **2004**, *237*, 348−351.
(53) Rosa, E. D. l.; Sepulveda-Guzman, S.; Reeja-Jayan, B.; Torres, A.; Salas, P.; Elizondo, N.; Yacaman, M. J. Controlling the Growth and Luminescence Properties of Well-Faceted ZnO Nanorods. *J. Phys. Chem. C* **2007**, *2007*, 8489−8495.
(54) Rodriguez, J. A.; Maiti, A. Adsorption and Decomposition of H_2S on MgO (100), NiMgO (100), and ZnO (0001) Surfaces: A First-principles Density Functional Study. *J. Phys. Chem. B* **2000**, *104*, 3630−3638.
(55) Waltman, R. J.; Bargon, J. Electrically Conducting Polymers: A Review of the Electropolymerization Reaction, of the Effects of Chemical Structure on Polymer Film Properties, and of Applications towards Technology. *Can. J. Chem.* **1986**, *64*, 76−95.
(56) Garnier, F.; Tourillon, G.; Barraud, J. Y.; Dexpert, H. First evidence of Crystalline Structure in Conducting Polythiophene. *J. Mater. Sci.* **1985**, *20*, 2687−2694.
(57) Baeten, L.; Conings, B.; Boyen, H.-G.; D'Haen, J.; Hardy, A.; D'Olieslaeger, M.; Manca, J. V.; Bael, M. K. V. Towards Efficient Hybrid Solar Cells Based on Fully Polymer Infiltrated ZnO Nanorod Arrays. *Adv. Mater.* **2011**, *23*, 2802−2805.
(58) Poverenov, E.; Li, M.; Bitler, A.; Bendikov, M. Major Effect of Electropolymerization Solvent on Morphology and Electrochromic Properties of PEDOT Films. *Chem. Mater.* **2010**, *22*, 4019−4025.
(59) Schrebler, R.; Grez, P.; Cury, P.; Veas, C.; Merino, M.; Gomez, H.; Cordova, R.; del Valle, M. A. Nucleation and Growth Mechanisms of Poly(thiophene) Part 1. Effect of Electrolyte and Monomer Concentration in Dichloromethane. *J. Electroanal. Chem.* **1997**, *430*, 77−90.
(60) Greene, L. E.; Law, M.; Yuhas, B. D.; Yang, P. ZnO-TiO_2 Core-Shell Nanorod/P3HT solar cells. *J. Phys. Chem. C* **2007**, *111*, 18451−18456.
(61) Cowan, S. R.; Banerji, N.; Leong, W. L.; Heeger, A. J. Charge Formation, Recombination, and Sweep-Out Dynamics in Organic Solar Cells. *Adv. Funct. Mater.* **2012**, *22*, 1116−1128.
(62) Yassar, A.; Roncali, J.; Garnier, F. Conductivity and Conjugation Length in Poly(3-methylthiophene) Thin Films. *Macromolecules* **1989**, *22*, 804−809.
(63) Micaroni, L.; Dini, D.; Decker, F.; Paoli, M.-A. D. Electrosynthesis and Characterization of Poly(3-methylthiophene) on Different Substrates. *J. Solid State Electrochem.* **1999**, *3*, 352−356.
(64) Tsoi, W. C.; Spencer, S. J.; Yang, L.; Ballantye, A. M.; Nicholson, P. G.; Turnbull, A.; Shard, A. G.; Murphy, C. E.; Bradley, D. D. C.; Nelson, J.; Kim, J.-S. Effect of Crystallization on the Electronic Energy Levels and Thin Film Morphology of P3HT:PCBM Blends. *Macromolecules* **2011**, *44*, 2944−2952.
(65) Green, M. A. Solar Cell Fill Factors: General Graph and Empirical Expressions. *Solid-State Electron.* **1981**, *24*, 788−789.
(66) Lee, J. H.; Shin, J.-H.; Song, J. Y.; Wang, W.; Schlaf, R.; Kim, K. J.; Yi, Y. Interface Formation Between ZnO Nanorod Arrays and Polymers (PCBM and P3HT) for Organic Solar Cells. *J. Phys. Chem. C* **2012**, *116*, 26342−26348.
(67) Conings, B.; Baeten, L.; Boyen, H.-G.; D'Haen, J.; Bael, M. K. V.; Manca, J. V. Relation between Morphology and Recombination Kinetics in Nanostructured Hybrid Solar Cells. *J. Phys. Chem. C* **2012**, *116*, 14237−14242.